Carbon 125 (2017) 614–629

Contents lists available at ScienceDirect

Carbon

journal homepage: www.elsevier.com/locate/carbon

Structural analysis of hydrothermal char and its models by density functional theory simulation of vibrational spectroscopy

A.B. Brown [a], B.J. McKeogh [a], G.A. Tompsett [a], R. Lewis [b], N.A. Deskins [a], M.T. Timko [a, *]

[a] Department of Chemical Engineering, Worcester Polytechnic Institute, Worcester, MA 01609, USA
[b] Cabot Corporation, Billerica, MA, 01821, USA

ARTICLE INFO

Article history:
Received 25 July 2017
Received in revised form
13 September 2017
Accepted 14 September 2017
Available online 15 September 2017

ABSTRACT

Density Functional Theory (DFT) and experimental measurements were used to develop a systematic method for interpreting the Raman spectra of hydrothermal char (hydrochar). Average band locations, relative intensities, and their trends relative to structural features were determined for the G, D, and Kekulé bands. When combined with several other less prominent vibrational modes, including vibrations associated with aromatic, ether, alkyl, and carbonyl bonds, the calculated average locations reproduced all major features of hydrochar Raman spectra. Two model structures were found that could reproduce the main features of the hydrochar Raman spectrum and its elemental analysis: 1) a structure consisting of arene domains comprised of 6–8 rings connected via aliphatic chains or 2) a furan/arene structure consisting primarily of single furans and 2 or 3ring arenes. NMR confirmed that the furan/arene ratio of glucose hydrochar is approximately 1:1, consistent with the furan/arene structure supported by Raman spectra. This work establishes an interpretation method for hydrochar Raman spectra and reconciles the main features of hydrochar structures determined using Raman spectroscopy with those based on other methods.

© 2017 Elsevier Ltd. All rights reserved.

1. Introduction

Biochars [1] are carbonaceous materials made from the thermal decomposition of biomass and waste-derived carbon [2]. Biochars are potentially useful for a variety of applications, including water purification [3], soil amendment [4], catalysis [5], and gas storage [6]. Several recent reviews [7–9] establish the potential usefulness of biochar materials. For example, Wei et al. [10] synthesized biochars from cellulose and activated them with a KOH treatment to prepare activated carbons with surface areas as great as 2967 $m^2\ g^{-1}$ (nitrogen sorption). These activated carbons were used to make carbon electrodes with a specific capacitance of 236 $F\ g^{-1}$ (100 $F\ cm^{-3}$) at a sweep rate of 1 $mV\ s^{-1}$. Similarly, Regmi et al. [11] converted switch grass into activated carbon by using a two-step process consisting of carbonization and KOH activation. The cadmium capacity of the resulting material was reported to be 34 $mg\ g^{-1}$, compared to 1.5 $mg\ g^{-1}$ for commercially available activated carbon (Calgon WPH).

Biochars can be divided into two categories, pyrolysis chars and hydrothermal chars (which we will refer to as “hydrochar”). Hydrochars are differentiated from pyrolysis biochars by the presence of a bulk water phase during their synthesis; hence, the synthesis process itself is termed “hydrothermal carbonization” or HTC [12]. Since many biorenewable feedstocks have high moisture content (for example, municipal waste [13] and many agricultural residues [14]), the energy efficiency of HTC can be greater than that of pyrolysis [15], a process which requires a dried feedstock [16]. Also, the physical and chemical composition of hydrochar is distinct from pyrolysis biochar [17], a factor which may be beneficial for specific applications [17]. For example, Liu et al. [18] compared the composition and performance of pinewood biochars synthesized under both hydrothermal and pyrolytic conditions. Interestingly, Liu et al. [18] reported that the pyrolysis chars possessed greater surface areas than the hydrochar (29 $m^2\ g^{-1}$ for pyrochar to 21 $m^2\ g^{-1}$ of hydrochar) as well as a significantly larger meso and macropore volume (0.89 $cm^3\ g^{-1}$ for pyrochar and 0.05 $cm^3\ g^{-1}$ for hydrochar). Despite having greater surface area, the copper adsorption capacity of the pyrolysis chars was less than that of the hydrochar (2.73 $mg\ g^{-1}$ for pyrochar and 4.21 $mg\ g^{-1}$ for hydrochar), a difference the authors attributed to the greater oxygen content of the hydrochar (35%) compared to the pyrolysis char (4%)

* Corresponding author.
E-mail address: mttimko@wpi.edu (M.T. Timko).

https://doi.org/10.1016/j.carbon.2017.09.051
0008-6223/© 2017 Elsevier Ltd. All rights reserved.

[18].

The molecular composition of hydrochar remains the subject of debate. Fig. 1 shows 3 model hydrochar structures proposed by Sevilla et al. [19], Latham et al. [20], and Chuntanapum et al. [21], respectively. The models clearly have some consistent features, namely the presence of aromatic rings and oxygen functional groups. However, important differences are also apparent, including differences in the types of aromatic ring (arene vs. furan), presence or absence of cyclic alkanes, and the number of rings present in fused aromatic structures. An accepted molecular model for hydrochar would help guide technological efforts to utilize and tailor hydrochar for specific applications.

Some of the differences in hydrochar model structures are attributable to inherent differences in the different methods used for structural analysis. Hydrochar has been examined using methods that capture primarily elemental composition [5] (for instance, combustion and atomic spectroscopy), functional group content [22–24] (including NMR, C-XANES, and vibrational spectroscopy), or physical/textural properties (nitrogen/carbon dioxide sorption and electron microscopy). The hydrochar models shown in Fig. 1a [19] and 1c [21] were based primarily on IR and Raman spectroscopy; these techniques suggest that hydrochar is a highly defective graphitic structure with significant oxygen functional group substitution. Fig. 1b was based on C-XANES measurements of hydrochar, a method which indicates that the structure is composed primarily of individual furanic rings [20]. Similarly, Baccile et al. [25] used NMR analysis to propose furan rings as the main repeat unit in hydrochar. While differences in synthesis conditions (temperature, residence time, starting reactant) may play a role in the differences between model structures [26], different experimental techniques clearly provide conflicting information that leads to inference of different structures.

NMR and Raman spectra are two of the most common methods used for carbon material characterization. NMR analysis of hydrochars benefits from several inherent advantages, most notably that it allows nuclei-nuclei cross correlation analysis and spectral editing that can help clarify assignments [27]. On the other hand, Raman scattering has advantages of rapid sample preparation and scan times (minutes compared to hours for NMR) and is particularly sensitive to C—C bonds [28]. In fact, Raman scattering has been useful for characterization of graphene and graphite structures [29,30], and has recently been carefully studied as a tool for characterization of pyrolysis chars [31]. Unfortunately, the information that Raman spectroscopy can provide for analysis of hydrochars is limited largely due to their complex Raman spectra that apparently consists of many overlapping bands [32]. Careful study of hydrochar Raman spectra is required to increase the usefulness of this tool for hydrochar characterization and resolve apparent differences between model structures based on Raman spectroscopy from those determined by other methods.

Several authors have previously suggested methods to interpret the Raman spectra of disorganized carbon materials [28,32–41]. For example, Ferrari et al. [33], suggested that the Raman spectra of highly graphitic carbons could be characterized as consisting primarily of 2 distinctive bands, a “G band”, generally appearing at 1580 cm^{-1}, and a “D band”, generally appearing at 1350 cm^{-1}. Tuinstra et al. [35] established the origin of the G band to be defect-free graphene sheets, an assignment that remains generally accepted. The D band is typically attributed to the C=C vibrations of defects in the graphene sheets [35–37]. Furthermore, Tuinstra et al. [35] originally attributed the D band to particle size or edge effects, suggesting that the symmetric A_{1G} mode of the graphene lattice becomes active at the particle boundary. Ferrari [36] later refined the attribution of the D band in graphitic carbons, demonstrating that the intensity and width of the D band were greatest at the edges of a graphene sheet. As a further refinement, Castiglioni et al. [37] suggested that the D band originates from activation of phonons in sp^2 domains around the edge of aromatic rings or defects in the graphitic lattice.

Hydrochar Raman spectra universally exhibit characteristic bands in the same wavenumber range as is typical of D and G bands [42,43]. However, while the G and D band assignments for graphite are straightforward, the distinction between the basal plane and the edge is not well-defined for even the largest PAH sub-units thought to comprise hydrochar (see Fig. 1). Furthermore, while graphite Raman spectra consist of narrow G and D bands (<20 cm^{-1}), the hydrochar G and D bands are broad (>50 cm^{-1}). Likewise, Raman spectra of graphitic materials are typically dominated by a major G band, with only a minor D band, so that the G/D intensity ratio of graphitic materials is typically greater than 10. In contrast with graphite, the G/D intensity ratio of hydrochars is only about 2. Lacking a better alternative, many authors generally interpret observed hydrochar spectra as suggesting a defect-rich graphitic material, even though the graphitic content in hydrochar is generally accepted to be negligible [22,44].

Based on their analysis of the Raman spectra of defect-rich carbonaceous materials (primarily soot), Sadezky et al. [39] and Beyssac et al. [28] suggested an approach that was more comprehensive than the traditional G/D band assignment. The new assignment [28] contains a G band at 1580 cm^{-1} and sub-divides the D band into 4 sub-bands, each associated with specific structural defects. This method has been applied by other research groups analyzing carbonaceous materials [40], but it was derived primarily for soot and other low oxygen content carbonaceous

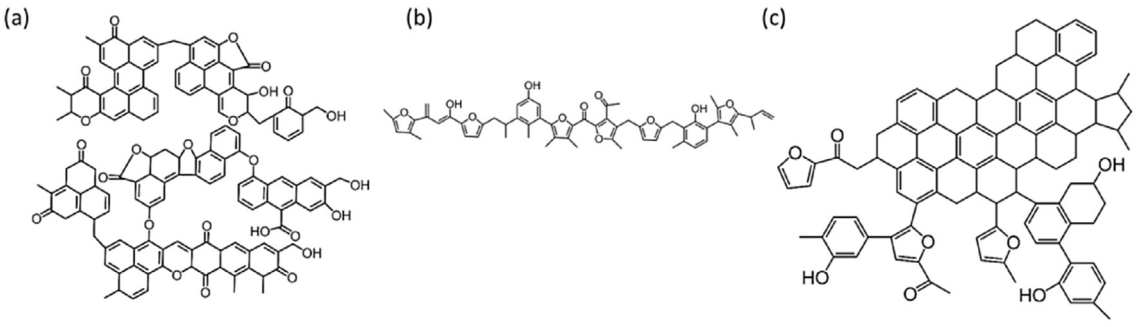

Fig. 1. Hydrochar models reported in the literature: Data from the following sources: Structure (a) is reprinted (adapted) with permission from Sevilla et al. [19]. Copyright© 2009; John Wiley & Sons; structure (b) is reprinted from Carbon, 114, Kenneth G.Latham et al., Synchrotron based NEXAFS study on nitrogen doped hydrothermal carbon: Insights into surface functionalities and formation mechanisms, 566-578, Copyright (2017), with permission from Elsevier; Structure (c) is reprinted (adapted) with permission from Chuntanapum and Matsumura [21]. Copyright© 2009; American Chemical Society).

Download English Version:

https://daneshyari.com/en/article/5431724

Download Persian Version:

https://daneshyari.com/article/5431724

Daneshyari.com